

## Synthesis and characterization of zirconia nanorods as a photo catalyst for the degradation of methylene blue dye

R. Jeba<sup>1,4,a</sup>, S. Radhika<sup>2,4</sup>, C. M. Padma<sup>3,4</sup>, X. Ascar Davix<sup>5</sup>

<sup>1</sup>Research Scholar, Women's Christian College, Tamilnadu, India

<sup>2</sup>Pioneer Kumaraswamy College, Tamilnadu, India

<sup>3</sup>Department of Physics, Women's Christian College, Tamilnadu, India

<sup>4</sup>Manonmaniam Sundaranar University, Abishekapatti, Tirunelveli, Tamilnadu, India

<sup>5</sup>Department of Electronics and Communication Engineering, R.V.R. & J.C. College of Engineering, Andhra Pradesh, India

<sup>a</sup>jeba170787@gmail.com

Corresponding author: R. Jeba, jeba170787@gmail.com

**ABSTRACT** t-ZrO<sub>2</sub> nano crystalline photocatalyst have been synthesized by a simple co-precipitation method. The crystal structure, morphology, size, and elemental composition of ZrO<sub>2</sub> nanorods were determined using XRD, SEM, EDX analysis. The optical properties and photocatalysis were analyzed using UV-Vis spectroscopy. The investigation of XRD pattern indicates tetragonal (t-ZrO<sub>2</sub>) and monoclinic phases (m-ZrO<sub>2</sub>) for the annealing temperatures 500 and 900 °C respectively. SEM images depicts rod like morphology. UV-Vis spectra illustrates that the synthesized samples have wide band gap. t-ZrO<sub>2</sub> photocatalyst degrades methylene blue dye with 80 % removal efficiency in 180 minutes.

**KEYWORDS** zirconium oxide (ZrO<sub>2</sub>), co-precipitation, photocatalysis

**FOR CITATION** Jeba R., Radhika S., Padma C.M., Ascar Davix X. Synthesis and characterization of zirconia nanorods as a photo catalyst for the degradation of methylene blue dye. *Nanosystems: Phys. Chem. Math.*, 2022, **13** (1), 78–86.

### 1. Introduction

In the current decade, industrialization is rapidly increasing all over the world. The increase in industries leads to the contamination of water. The main cause for water contamination is the waste effluents from chemical, textile, medicine, manufacturing, and petroleum industries [1]. Important organic compounds which contaminate groundwater resources are dyes, pesticides, aromatic solvents. These organic compounds affect the aquatic life and human health. Most of the contaminations are removed using conventional wastewater management systems [2, 3]. Around 700,000 tons of dyes were produced annually for industrial purpose. Dyes used by the textile industry are one important factor which affects the aquatic life [4]. To prevent the contaminations of water and conserve the aquatic ecosystem, there is the need for the research of wastewater treatment options such as coagulation, flocculation, precipitation, adsorption, ion exchange and membrane processing. Advanced Oxidation Process (AOP) is one fundamental water treatment method which has been efficiently developed. AOP is performed at room temperature and normal pressure. A hydroxyl radical is created on the catalyst surface which then acts as oxidizing agent for the decontamination of water [5]. Photocatalysis is a phenomenon in which the valance band electrons are excited into the conduction band when a semiconducting material absorbs a light that is higher than its energy band gap value [27]. Various semiconductor nano metal oxides such as TiO<sub>2</sub>, ZnO, SnO<sub>2</sub>, have been studied for their photocatalytic ability to degrade pollutants [6]. N-type semiconductor Zirconia has also been used as a photocatalyst [7, 8]. An attempt has been made to investigate the photo degradation of methylene blue (MB) dye using zirconium oxide.

Zirconia is the most popular ceramic oxide used in a variety of applications such as engineering, science and medical fields. The important properties of zirconia are high density, high fracture toughness, high temperature capability and low thermal conductivity [9]. Because of its photochemical stability, high refractive index, large band gap, transparency in the visible and near-infrared regions of the spectrum, and low phonon energy, zirconia is the best optical medium for lanthanide ions among p-type semiconductors. It also has a low phonon energy, which reduces the likelihood of non-radiative transitions due to multiphonon relaxation [31]. Zirconia (ZrO<sub>2</sub>) has a high bandgap energy and is a chemically stable material. It exhibits more oxygen vacancies on its surface. Since it has high ion exchange capacity and redox activities, it is used as a photocatalyst. The optical photon energy of zirconia relies on its crystalline structure. This enhances the light absorption ability and charge separation due to the surface modification, which increases the photocatalytic ability. Zirconia is polymorphic, and shows different phases at different temperatures. Also, it shows three crystal

structures, namely tetragonal, monoclinic and cubic. Zirconia was used in monoclinic phase which was stable at temperature  $T < 1170$  °C. The stable properties of this material are not consistent at room temperature. The phase stability mainly depends on the preparation of the material [10]. The material was prepared at various temperatures and also in three different phases [11, 12]. Tetragonal  $ZrO_2$  was formed at 700 °C by co-precipitation method and it was formed at the same temperature by a microemulsion refined precipitation technique [13]. Only few researchers have reported on the photocatalytic activity of  $ZrO_2$  [20].  $ZrO_2$  nanoparticles played a major role in the area of photocatalysis with the amalgamation of other visible light active semiconductors.  $ZrO_2$  has negative flat band potential and wide band gap. The conduction band has the lowest potential and the valance band has the highest potential. The reduction potential of  $e^-$  in the conduction band was more negative than potentials of  $H_2/H_2O$  and  $CO/CO_2$ . Due to this, the oxidation potential of  $H^+$  in the valance band was more positive than the potential of  $O_2/H_2O$ . This property of  $ZrO_2$  makes it a better photocatalyst [28]. Zheng et al. synthesized Nanocrystalline  $ZrO_2$  by the L-lysine-assisted hydrothermal method and the photocatalytic activity was studied using Rhodamine B (Rh B) as a model pollutant [21]. Olga Długosz et al. proposed  $ZrO_2$ -ZnO nanoparticles for the degradation of MB solution. Since ZnO has broad energy gap, it limits the photocatalytic property. To enhance the photocataytic efficiency,  $ZrO_2$ -ZnO nanoparticles were used [22].

In this research article, zirconia ( $ZrO_2$ ) nanoparticles are synthesized by co-precipitation method under various annealing temperatures such as 500, 700, and 900 °C. The obtained nanoparticles are characterized by XRD, UV-vis, EDX and stockticker SEM analysis. Photocatalytic activity of synthesized  $ZrO_2$  nanoparticles on the degradation of MB is analyzed. MB is a phenothiazine derivative, used for dyeing textiles, and it is highly toxic and carcinogenic. An oxidation process is frequently required to degrade contaminants. Thus, we have chosen MB for the degradation process [29].

## 2. Materials and method

Nanorods of  $ZrO_2$  are prepared by simple co-precipitation method. An aqueous solution of zirconium oxychloride and sodium hydroxide were taken in the ratio of 0.5:2 M (8.056 g  $ZrOCl_2$ : 4 g NaOH /50 ml distilled water) to maintain a pH 12. Aqueous solution of zirconium oxychloride was magnetically stirred at 60 °C. NaOH solution was added dropwise to adjust to pH 12 and stirred constantly for 2 hours at 60 °C. The presence of chloride and sodium ions in the final product were controlled by filtering the obtained precipitate followed by repeatedly washing with distilled water and then finally with acetone. Thereafter the precipitate was dried at 150 °C by using a hot air oven. After drying the obtained precipitate was ground by using mortar and pestle to afford a fine powder. The  $ZrO_2$  thus obtained was divided into three parts. One part was annealed at 500 °C, another at 700 °C, and the third part at 900 °C for 2 hours.

X-Ray Diffraction (XRD) analysis with an XPERT-PRO diffractometer was used to determine the crystallite size and proper phases that exist in the zirconia nanorods in the diffraction angle  $2\theta$  ranging from 10 to 80°. Optical properties are analyzed using UV-VIS spectrum taken from Perkin Elmer Lambda 35 spectrophotometer. The photocatalytic activity of synthesized  $ZrO_2$  nanoparticles annealed at 500 °C on the degradation of MB was analyzed. An aqueous solution of MB (0.1 M, 50 ml) was taken and 0.2 g of the photocatalyst was suspended in that solution. The experiment was done under UV light irradiation. The continuously stirred solution was irradiated with a 50 W halogen lamp. For every 60 min, 4 ml of dye solution was taken from the system and the dye removal efficiency was analyzed by a UV-Vis spectrometer.

## 3. Results and discussion

UV-VIS spectrum taken from Perkin Elmer Lambda 35 spectrophotometer describes the absorbance and transmittance properties of zirconia nanorods and is also used to study the removal efficiency of the photocatalyst. Scanning Electron Microscope (SEM) images and EDAX analysis of the nano zirconia is characterized using EV018 (CARL ZEISS) and Quantax 200 with X Flash 6130 microscope.

### 3.1. Crystallinity, phase and structural studies

The wide band gap zirconia nanorods were synthesized using a co-precipitation method. The XRD pattern of the initial powder for zirconia nanoparticles is shown in Fig. 1 and identified amorphous state of the particle. The peaks at 32, 48, and 57 are in good accord with the standard JCPDS no. 87-2105 and are indexed as orthorhombic  $ZrO_2$ . The element is annealed at various temperatures and examined to obtain a definite structure. The X-ray diffraction pattern obtained for  $ZrO_2$  nanoparticles annealed at 500, 700 and 900 °C are shown Fig. 2. The XRD pattern was used to identify the phase of nanoparticles and it confirmed pure tetragonal phase (JCPDS-50-1089) for zirconia annealed at 500 °C. The peaks are indexed as follows: 30.24° (011), 34.97° (002), 35.31° (110), 50.59° (112), 59.92° (013), 63.04° (202) and 74.34° (220). The average crystallite size of the sample at 500 °C was 29.74 nm.

The XRD pattern of  $ZrO_2$  annealed at 700 °C confirms both tetragonal and monoclinic phases. The phase composition at 700 °C consists of 87 % monoclinic and 13 % tetragonal phases.

The highest peak in the pattern is indexed as tetragonal phase (JCPDS-50-1089) corresponding to the angle 30.3° (011). The remaining peaks are indexed as the monoclinic phase (JCPDS-65-1025). The major peaks of the monoclinic phase are 50.67° (122), 50.21° (220), 60.08° (302), 28.28° (111), and 59.88° (131). The average crystallite size of the sample at 700 °C is 42.5 nm.

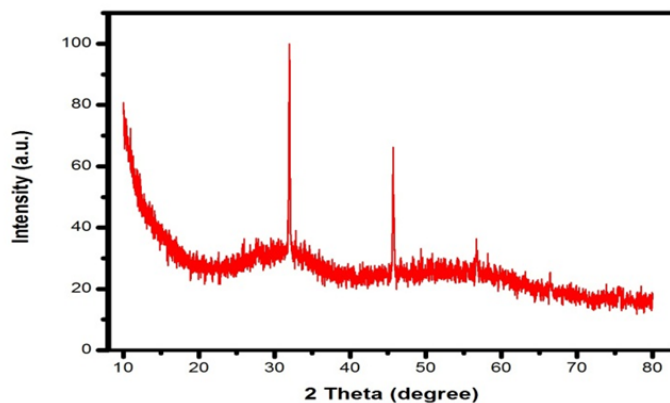
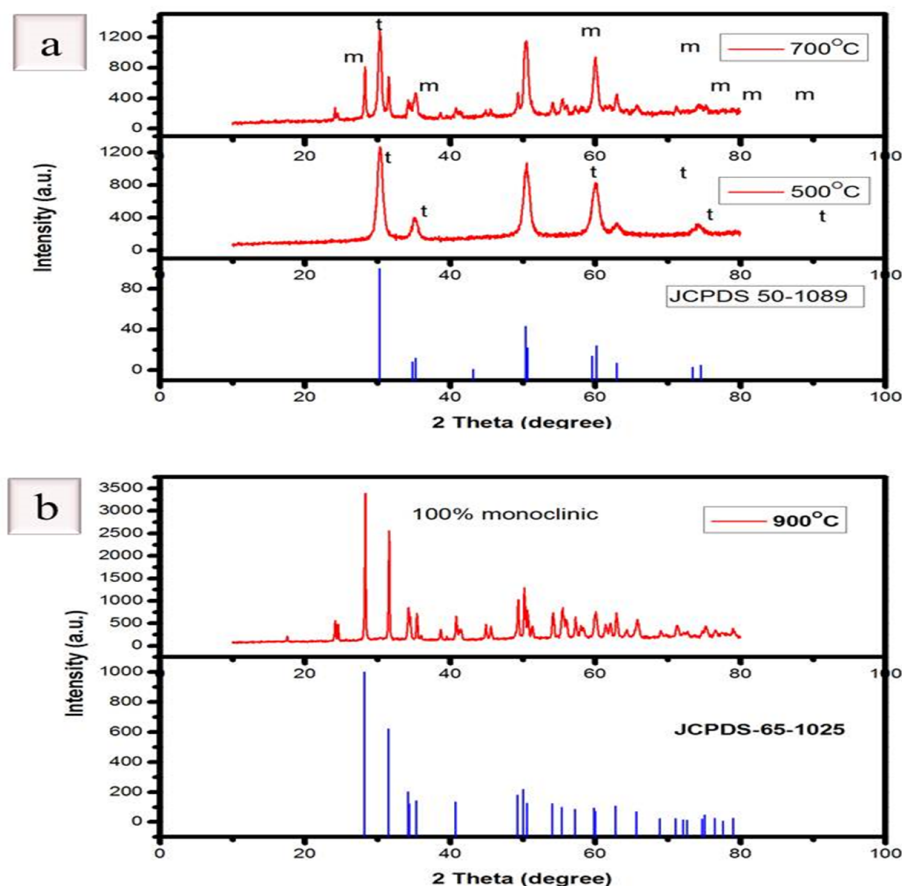


FIG. 1. XRD pattern of as prepared sample

FIG. 2. XRD pattern of  $\text{ZrO}_2$  calcined at (a) 500 °C and 700 °C, (b) 900 °C

The peaks of the XRD pattern of  $\text{ZrO}_2$  annealed at 900 °C are indexed as monoclinic phase (JCPDS-65-1025). The major peaks of the monoclinic phase are 28.30° ( $\bar{1}11$ ), 31.59° (111), 50.24° (220), 49.39° (022), and 34.24° (020). The average crystallite size of the sample at 900 °C is 63.84 nm. The average crystallite size, phase and energy gap parameters of  $\text{ZrO}_2$  with various annealing temperature are listed in Table 1. The XRD patterns of all three samples reveal that the tetragonal phase is transformed into the monoclinic as the annealing temperature is increased from 500 to 900 °C. The faster phase transformation is due to the increase of calcination temperature [23, 24].

Annealing temperature has a significant role on the structural modification of the nanoparticles. It was observed that the crystallite size increased with increasing temperature. Generally, calcination decreases the lattice defects and strains; however, on the other hand, higher temperatures may cause crystallites to coalesce, which leads to an increase in the crystallite and nanoparticle sizes [26]. The average crystallite size ( $D$ ) of  $\text{ZrO}_2$  powder was calculated using Scherrer's formula,  $D = \frac{0.9\lambda}{\beta \cos \theta}$ , where,  $\lambda$  is the wavelength of the X-rays;  $\theta$  is the Bragg's diffraction angle, and  $\beta$  is the full width

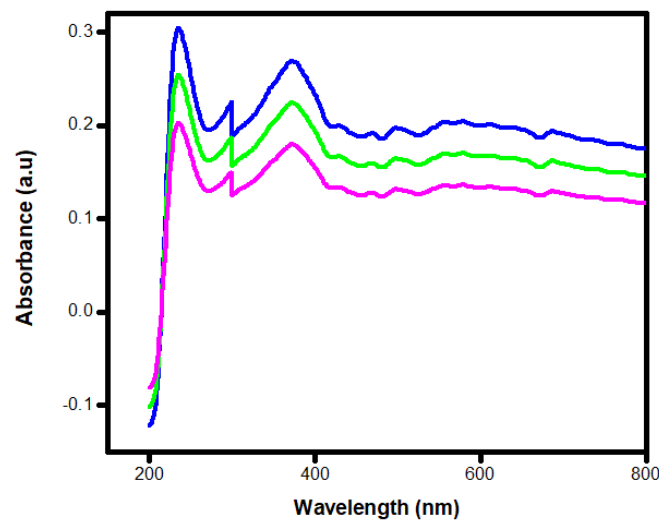
TABLE 1. The average crystallite size, phase and energy gap parameters of ZrO<sub>2</sub> with various annealing temperatures

Annealing temperature	Average Crystallite size, $D$ (nm)	Phase	Energy gap parameters, eV	
			$E_{g1}$	$E_{g2}$
500 °C	29.74	t	4.7	4.6
700 °C	36.09 (t) 50.45 (m)	t + m	4.6	4.4
900 °C	63.84	m	4.4	4.3

at half maximum (FWHM) of the diffraction peaks (in radians) [30, 33]. The diffraction pattern shows sharp and well defined peaks, which indicate the highly crystalline nature as well as purity of the sample [14].

### 3.2. Optical studies

Figure 3 shows the optical absorbance spectrum of ZrO<sub>2</sub> at different annealing temperatures such as 500, 700, and 900 °C. The strong absorbance peak for ZrO<sub>2</sub> annealed at 500 and 700 °C occurs at 375.2 nm. The strong absorbance peak occurs at 278.6 nm, for the sample prepared at 900 °C. So it is noted that, the absorbance increases when the annealing temperature increases.

FIG. 3. Optical absorbance spectrum of ZrO<sub>2</sub> at different calcination temperatures

The band gap energy of the prepared samples is calculated by using Tauc relation:

$$\alpha h\nu = A(h\nu - E_g)^n, \quad (1)$$

where,  $h\nu$  is the energy of photon,  $E_g$  is the band gap energy,  $A$  is the proportionality constant,  $n$  takes the value 1/2 for direct allowed transitions and  $\alpha$  is the absorption coefficient [15]. The absorption coefficient  $\alpha$  is determined using the formula:

$$\alpha = \frac{2.303 \log(1/T)}{t}, \quad (2)$$

Here,  $T$  represents transmittance and  $t$  represents the thickness of sample ( $t = 1$  mm) [16]. The Tauc plot is drawn to determine the band gap of ZrO<sub>2</sub> at different annealing temperatures and it is shown in Fig. 4. It is identified that, the variation of  $(\alpha h\nu)^2$  with respect to  $h\nu$  is linear which reveals the transition is a directly allowed transition. The band gap energy was calculated from the x-axis intersection point of the linear fit of the Tauc plot. The band gap energy of ZrO<sub>2</sub> at different annealing temperature was determined from the Tauc plot and is listed in Table 1.  $E_g$  values of the synthesized nanostructures are found from 4.3 to 4.7 eV.

The energy gap of ZrO<sub>2</sub> decreases with respect to an increase in the temperature. This is due to the increased crystallite size, increased inter-atomic space and surface defect such as oxygen vacancies [24]. The variation of electronic levels that arises between the conduction band and valance band is due to the presence of oxygen vacancies [25].

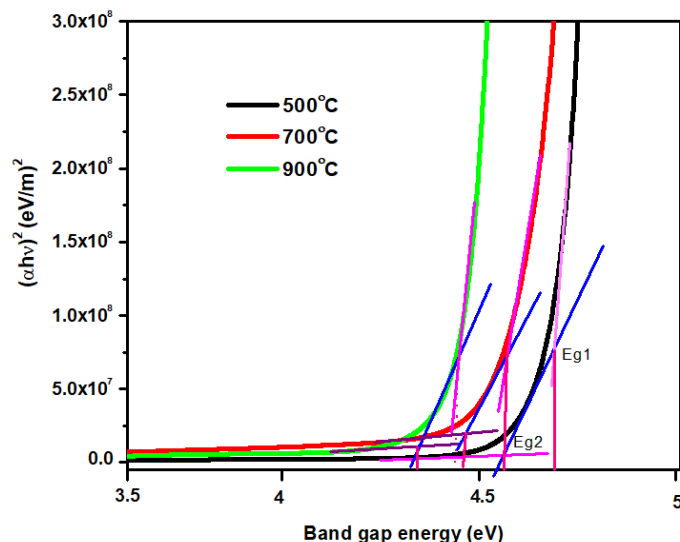


FIG. 4. Tauc's plot of  $ZrO_2$  at different annealing temperatures to determine the band gap energy

### 3.3. SEM and EDX analysis

The morphology of the synthesized  $ZrO_2$  nanoparticles at 500, 700, and 900 °C was analyzed with scanning electron microscopy (SEM) taken at different magnification scales, and the results are shown in Fig. 5. The synthesized samples were observed to have a rod-shaped morphology. The first stage of the growth of nanorod is isotropic which has the growth of seed particles. The second stage of the growth is anisotropic which has the growth in one direction. The third stage of the growth is rod shaped particle. The approximate values of the average lengths and widths of the nanorods at 500, 700, and 900 °C are 222, 159, 102 nm and 31, 14, 17 nm respectively.

The EDX characterization depicts the elemental composition of the prepared  $ZrO_2$  nanoparticles at 500, 700, and 900 °C. The EDX characterization spectrum is shown in Fig. 6. High intense peak was identified for zirconium (Zr) and oxygen (O) elements. These results are also in agreement with the SEM-EDX mapping images shown in Fig. 7. Furthermore, these images confirm that Zr and O elements are homogeneously dispersed.

### 3.4. Photocatalytic performance

The photocatalytic performance of the prepared catalyst  $ZrO_2$  was experimentally determined by the degradation of MB organic dye. The optical absorbance spectra of the degradation of MB dye using  $ZrO_2$  nanoparticles annealed at 500 °C is shown in Fig. 8. An aqueous solution of MB (0.1 M, 50 ml) was taken and 0.2 g of photocatalyst zirconia was added. The experiment was done under UV irradiation at 350 nm. The solution is exposed to halogen lamp of 50 W with continuous stirring. For every 60 min, 4 ml of dye solution is taken from the system and the degradation percentage is analyzed by UV-Vis spectrophotometer. From the absorbance spectrum, the strong peak is identified at 663.25 nm which is the absorption wavelength of MB dye. The following equation provides the removal efficiency ( $E$ ) of MB degradation:

$$E = \frac{C_0 - C}{C_0} \times 100 \%, \quad (3)$$

where  $C_0$  is the initial concentration of dye and  $C$  is the concentration of MB after UV irradiation. It was observed that, 53 % of MB dye degraded after 1 hour and 80 % of MB dye was degraded after 3 hours. This is mainly due to high crystallinity nature of  $t-ZrO_2$  prepared at 500 °C, small crystallite size and well defined morphology and surface properties. The normalized residual concentration of MB dye is estimated using:

$$\frac{C_t}{C_0} = \frac{A_t}{A_0},$$

where  $C_0$  and  $C_t$  are the initial and residual concentration of MB dye,  $A_t$  and  $A_0$  are the absorbance intensity at time  $t$  and at time  $t = 0$  obtained from UV-absorbance spectrum [17].

The growth of the rod shaped particle is greater in one direction with respect to the growth of the particle in other dimensions [18]. Since, the morphology of the prepared nanoparticle is rod shape; the surface area of the particle is high. The high surface area provides more active sites for the reaction of photodegradation [19]. Due to this property, the efficiency of the degradation of MB is high for zirconia even though it has wide band gap. The decomposition of MB dye by  $ZrO_2$  with respect time is shown in Fig. 9. In addition to particle size, phase composition, and optical characteristics, there may be other parameters that influence photocatalytic activity [32].

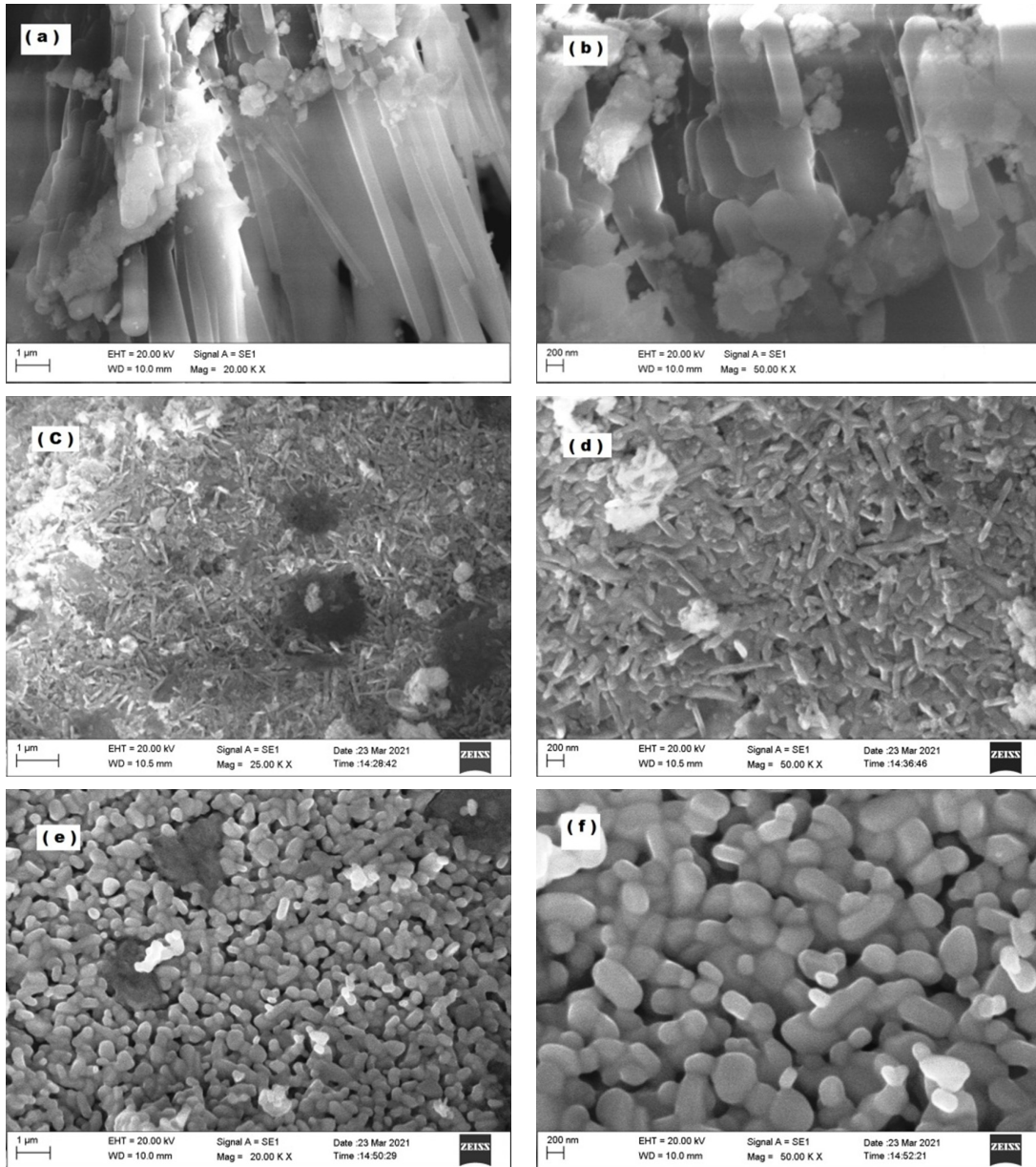


FIG. 5. SEM image of ZrO<sub>2</sub> at (a), (b) 500 °C, (c), (d) 700 °C and (e), (f) 900 °C

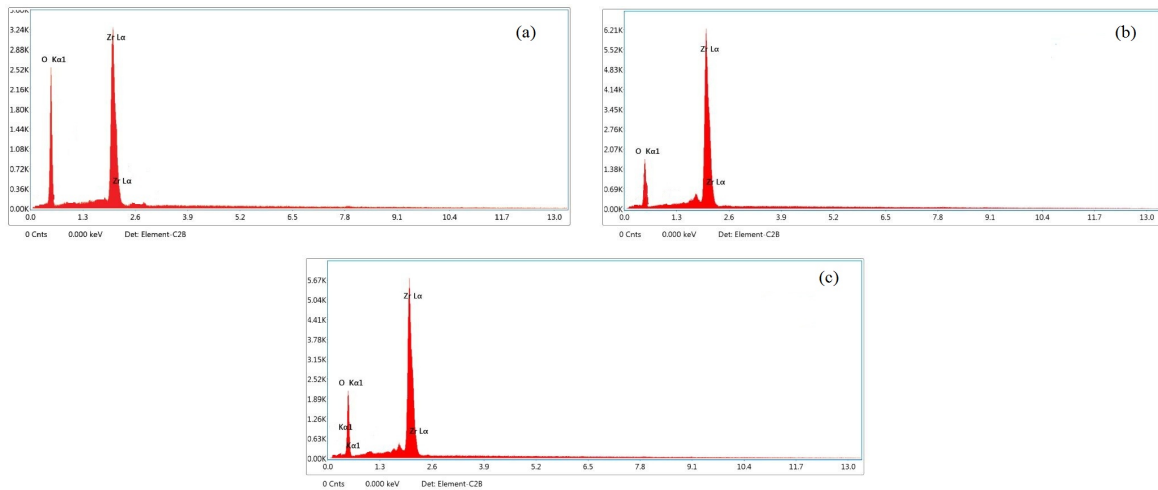


FIG. 6. EDX characterization spectra of ZrO<sub>2</sub> at (a) 500 °C, (b) 700 °C, and (c) 900 °C

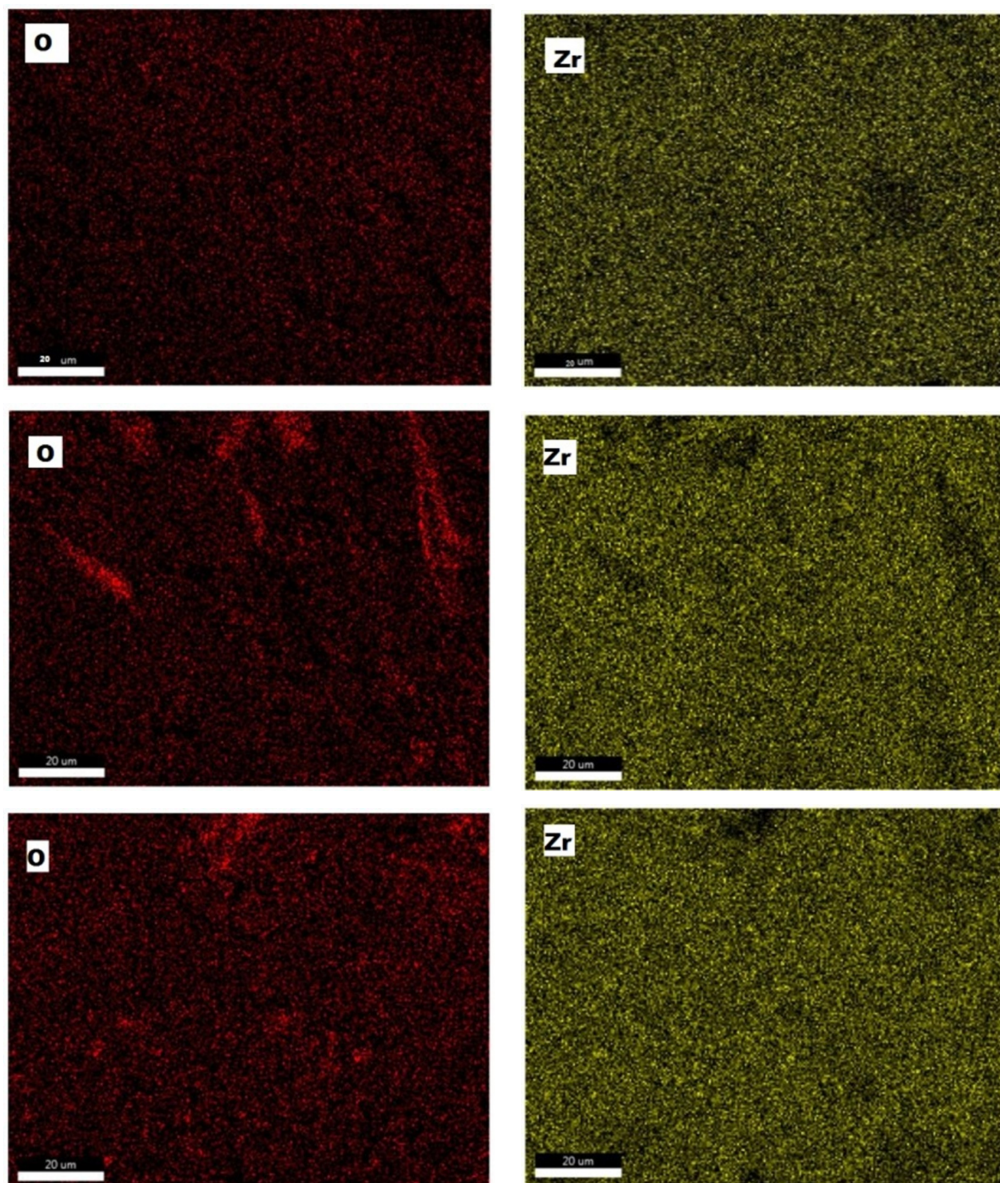


FIG. 7. EDX mapping of  $ZrO_2$  at (a) 500 °C, (b) 700 °C and (c) 900 °C

#### 4. Conclusion

Zirconium oxide nanorods have been successfully synthesized by a co-precipitation method under various annealing temperatures such as 500, 700, 900 °C. XRD analysis confirmed the tetragonal phase ( $t-ZrO_2$ ) at 500 °C. Both the tetragonal and monoclinic phases were present when annealed at 700 °C. The pure monoclinic phase ( $m-ZrO_2$ ) was identified at 900 °C. The crystallite size increased at higher annealing temperatures. The band gap energy was calculated from UV-Vis absorption spectrum and it was found to decrease with increases in annealing temperature. Rod shaped morphology was observed in SEM images, and therefore, the particles had high surface area. This enhances the removal efficiency of the photocatalyst. The elemental composition of the synthesized nanoparticles was found using EDX analysis. The nanoparticles synthesized at 500 °C provide small crystallite size and high crystallinity and rod shaped morphology and therefore used as photocatalyst for degradation of MB dye. This photocatalyst degrades 80 % of MB dye in 180 minutes under UV irradiation.

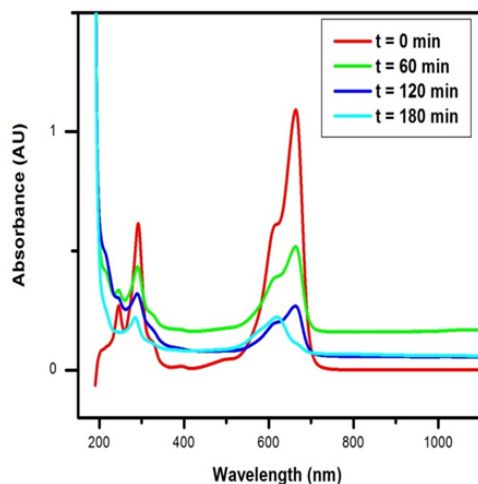


FIG. 8. Optical absorbance spectra of MB dye using  $ZrO_2$  at  $500\text{ }^\circ\text{C}$

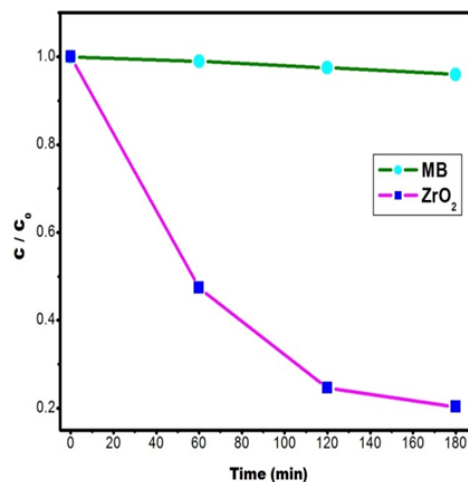


FIG. 9. Removal efficiency of  $ZrO_2$

## References

- [1] Mahy J.G., Lambert S.D., et al. Ambient temperature  $ZrO_2$ -doped  $TiO_2$  crystalline photocatalysts: Highly efficient powders and films for water depollution. *Materials Today Energy*, 2019, **13**, P. 312–322.
- [2] Sugi S., Usha Rajalakshmi P., Shanthi J. Photocatalytic Degradation efficiency of  $Cu_xZn_{1-x}O$  Composite. *Optik*, 2017, **131**, P. 406–413.
- [3] Scholz N. Setting Criteria on Endocrine Disruptors: Follow-Up to the General Court Judgment. Brief. From Eur. Parliam., 27 April 2016, P. 1–10.
- [4] Ratnayake S.P., Mantilaka M.M.M.G.P.G., et al. Carbon quantum dots-decorated nano-zirconia: A highly efficient photocatalyst. *Applied Catalysis A: General*, 2019, **570**, P. 23–30.
- [5] Oturan M.A., Aaron J.J. Advanced oxidation processes in water/wastewater treatment: principles and applications. A review. *Critical Reviews in Environmental Science and Technology*, 2014, **44** (23), P. 2577–2641.
- [6] Wang J., Gu H. Novel metal nanomaterials and their catalytic applications. *Molecules*, 2015, **20** (9), P. 17070–17092.
- [7] Kirsch B.L., Tolbert S.H. Stabilization of Isolated Hydrous Amorphous and Tetragonal Zirconia Nanoparticles through the Formation of a Passivating Alumina Shell. *Adv. Funct. Mater.*, 2003, **13**, P. 281–288.
- [8] Rashad M.M., Baioumy H.M. Effect of thermal treatment on the crystal structure and morphology of zirconia nanopowders produced by three different routes. *J. Mater. Process. Technol.*, 2008, **195**, P. 178–185.
- [9] Ward D.A., Ko E.I. Synthesis and structural transformation of zirconia aerogels. *Chem. Mater.*, 1993, **5**, P. 956–969.
- [10] Trice R.W., Su Y.J., Mawdsley J.R., Faber K.T. Effect of heat treatment on phase stability, microstructure, and thermal conductivity of plasma-sprayed YSZ. *J. Mater. Sci.*, 2002, **37**, P. 2359–2365.
- [11] Neppolian B., Wang Q., Yamashita H., Choi H. Synthesis and characterization of  $ZrO_2$ - $TiO_2$  binary oxide semiconductor nanoparticles: Application and interparticle electron transfer process. *Appl. Catal. A: Gen.*, 2007, **333**, P. 264–271.
- [12] Wu C., Zhao X., et al. Gas-phase photo-oxidations of organic compounds over different forms of zirconia. *J. Mol. Catal. A: Chem.*, 2005, **229**, P. 233–239.
- [13] Rajababu C. Influence of calcination temperature on structural, optical, dielectric properties of nano zirconium oxide. *Optik*, 2016, **127** (11), P. 4889–4893.
- [14] Besky Job C., Shabu R., Paul Raj S. Growth, structural, optical, and photo conductivity studies of potassium tetra fluoro antimonite. *Optik*, 2016, **127** (8), P. 3783–3787.
- [15] Radhika S., Padma C.M., Ramalingom S., Chithambara Thanu T. Growth, optical, thermal, mechanical and dielectric studies of potassium sulphate crystals doped with urea. *Archives of Physics Research*, 2013, **4** (1), P. 49–59.
- [16] Sadeghzadeh-Attar A. Efficient photocatalytic degradation of methylene blue dye by  $SnO_2$  nanotubes synthesized at different calcination temperatures. *Solar Energy Materials and Solar Cells*, 2018, **183**, P. 16–24.
- [17] Sheeba J.R., Radhika S., Padma C.M. Photo catalytic degradation of Methylene Blue Dye by Cu doped  $SnO_2$  Nano Crystals. *Wutan Huatan Jisuan Jishu*, 2020, **16** (9), P. 66–76.
- [18] Bilal A., Sachin K., Sumeet K., Animesh K. Ojha. Shape Induced (spherical, sheets and rods) Optical and Magnetic Properties of CdS Nanostructures with Enhanced Photocatalytic Activity for Photodegradation of Methylene Blue Dye under Ultra-violet Irradiation. *J. of Alloys and Compounds*, 2016, **679**, P. 324–334.
- [19] Vijaya Sankar K., Ashok M. Significantly enhanced photo catalytic activities of  $PbBi_2Nb_2O_9$ (Bulk)/ $TiO_2$ (Nano) hetero structured composites for methylene blue dye degradation under visible light. *Materials Chemistry and Physics*, 2020, **244**, 122659.
- [20] Venkata Reddy Ch., Bathula Babu, Neelakanta Reddy I, Jaesool Shim. Synthesis and Characterization of Pure tetragonal  $ZrO_2$  Nano Particles with enhanced Photocatalytic activity. *Ceramics International*, 2018, **44** (6), P. 6940–6948.
- [21] He Zheng, Kaiyu Liu, Huaqiang Cao, Xinrong Zhang. L-Lysine-Assisted Synthesis of  $ZrO_2$  Nanocrystals and Their Application in Photocatalysis. *J. Phys. Chem. C*, 2009, **113** (42), P. 18259–18263.
- [22] Długosz O., Szostak K., Banach M. Photocatalytic properties of zirconium oxide–zinc oxide nanoparticles synthesised using microwave irradiation. *Applied Nanoscience*, 2020, **10**, P. 941–954.
- [23] Prasad K., Pinjari D.V., Pandit A.B., Mhaske S.T. Synthesis of zirconium dioxide by ultrasound assisted precipitation: Effect of calcination temperature. *Ultrasonics Sonochemistry*, 2011, **18** (5), P. 1128–1137.
- [24] Horti N.C., Kamatagi M.D., et al. Structural and optical properties of zirconium oxide ( $ZrO_2$ ) nanoparticles: effect of calcination temperature. *Nano Express*, 2020, **1** (1), 010022.

- [25] Berlin J., Sujathalekshmy S., et al. Effect of Mn doping on the structural and optical properties of ZrO<sub>2</sub> thin films prepared by sol–gel method. *Thin Solid Films*, 2014, **550**, P. 199–205.
- [26] Shirsath S.E., Kadam R.H., et al. Effect of sintering temperature and the particle size on the structural and magnetic properties of nanocrystalline Li<sub>0.5</sub>Fe<sub>2.5</sub>O<sub>4</sub>. *J. of Magnetism and Magnetic Materials*, 2011, **323** (23), P. 3104–3108.
- [27] Baytar O., Sahin O., Kilicvuran H., Horoz S. Synthesis, structural, optical and photocatalytic properties of Fe-alloyed CdZnS nanoparticles. *J. of Materials Science: Materials in Electronics*, 2017, **29** (6), P. 4564–4568.
- [28] Sayama K., Arakawa H. Photocatalytic Decomposition of Water and Photocatalytic Reduction of Carbon Dioxide over ZrO<sub>2</sub> Catalyst. *The J. of Physical Chemistry*, 1993, **97** (3), P. 531–533.
- [29] Vasiljevic Z., Dojcinovic M.P., et al. Photocatalytic degradation of methylene blue under natural sunlight using iron titanate nanoparticles prepared by a modified sol–gel method. *R. Soc. Open Sci.*, 2020, **7** (9), 200708.
- [30] Langford J.I., Wilson A.J.C. Scherrer after sixty years: A survey and some new results in the determination of crystallite size. *J. Appl. Cryst.*, 1978, **11**, P. 102–113.
- [31] Bugrov A.N., Smyslov R.Yu., et al. Phosphors with different morphology, formed under hydrothermal conditions on the basis of ZrO<sub>2</sub>:Eu<sup>3+</sup> nanocrystallites. *Nanosystems: Phys., Chem., Math.*, 2019, **10** (6), P. 654–665.
- [32] Kolesnik I.V., Lebedev V.A., Garshv A.V. Optical properties and photocatalytic activity of nanocrystalline TiO<sub>2</sub> doped by 3d-metal ions. *Nanosystems: Phys., Chem., Math.*, 2018, **9** (3), P. 401–409.
- [33] Lele S., Anantharaman T.R. Influence of crystallite shape on particle size broadening of Debye-Scherrer reflections. *Proc. Indian Acad. Sci.*, 1966, **64**, P. 261–274.

---

Submitted 9 June 2021; revised 6 October 2021; accepted 1 February 2022

*Information about the authors:*

*Rengaswamy Jeba* – Research Scholar, Reg. No. 18223282132002, Women’s Christian College, Tamilnadu, India-629001; Manonmaniam Sundaranar University, Abishekapatti, Tirunelveli, Tamilnadu – 627012, India; ORCID 0000-0002-5156-0628; jeba170787@gmail.com

*Sathasivam Radhika* – Department of Physics, Pioneer Kumaraswamy College, Tamilnadu – 629003, India; Manonmaniam Sundaranar University, Abishekapatti, Tirunelveli, Tamilnadu-627012, India; radhisatha@yahoo.com

*Chellaia Muthammal Padma* – Department of Physics, Women’s Christian College, Tamilnadu – 629001, India; Manonmaniam Sundaranar University, Abishekapatti, Tirunelveli, Tamilnadu – 627012, India; padmajayaraj19@gmail.com

*Xavier Durai Ascar Davix* – Department of Electronics and Communication Engineering, R.V.R. & J.C. College of Engineering, Andhra Pradesh – 522019, India; ORCID 0000-0002-6795-7865; davixascar@gmail.com

*Conflict of interest:* the authors declare no conflict of interest.